QUANTUM CHEMISTRY

Quantum interference in atom-exchange reactions

Yi-Xiang Liu[1,2]†, Lingbang Zhu[1,2]†, Jeshurun Luke[1,2], J. J. Arfor Houwman[3,1], Mark C. Babin[1,2], Ming-Guang Hu[1,2]‡, Kang-Kuen Ni[1,4,2]*

Chemical reactions, in which bonds break and form, are highly dynamic quantum processes. A fundamental question is whether coherence can be preserved in chemical reactions and then harnessed to generate entangled products. Here we investigated this question by studying the 2KRb → K_2 + Rb_2 reaction at 500 nanokelvins, focusing on the nuclear spin degrees of freedom. We prepared the initial nuclear spins in KRb (potassium-rubidium) in an entangled state by lowering the magnetic field to where the spin-spin interaction dominates and characterized the preserved coherence in nuclear spin wave function after the reaction. We observed an interference pattern that is consistent with full coherence at the end of the reaction, suggesting that entanglement prepared within the reactants could be redistributed through the atom-exchange process.

Observing and exploiting quantum coherence in reactions has been a long-standing goal in chemistry. Coherence, often manifested through interference, has been observed in photoionization (*1*) and in inelastic and reactive scatterings involving light species such as hydrogen deuteride (HD), hydrogen fluoride (HF), and deuterium (D_2) in molecular beam experiments (*2*–*5*), in which comparison with full quantum-scattering calculations is needed to identify the signatures of interference. Coherence can also be leveraged to control the product-state distribution through interference between reaction pathways (*6*, *7*). Early experimental success has been shown in light-induced processes, such as photoassociation (*8*), photoionization (*9*), and photodissociation (*10*, *11*). However, experimental realization of controlled reactive scattering through the use of coherent interference remains elusive. A key underlying question is whether quantum coherence prepared in the reactants survives reactive bimolecular collisions, given the complex quantum dynamics involved. If coherence can be preserved, these chemical reactions may not only be controlled but also harnessed as a resource for quantum science.

To answer this question, we turned to ultracold molecular systems where exquisite control of the quantum state of molecules, which has been developed over the last two decades, allows for preparation in a single quantum state at microkelvin temperatures or lower (*12*–*18*). Specifically, we chose $^{40}K^{87}Rb$ bialkali molecules as our platform because the atom-exchange chemical reaction 2KRb → K_2 + Rb_2 has been observed (*19*) and studied extensively (*20*, *21*). Moreover, the product molecules K_2 and Rb_2 are homonuclear diatomic molecules, in which the bosonic potassium (K) and fermionic rubidium (Rb) nuclei have nuclear spins of $I_K = 4$ and $I_{Rb} = 3/2$ (where I is the angular momentum), allowing us to correlate their rotational states with nuclear spin states through the exchange symmetry of indistinguishable particles. To probe correlation of the reaction outcomes, it is crucial to identify the quantum states of products from individual events. For this purpose, we took advantage of a previously developed technique of coincidence detection, in which pairs of products were simultaneously and state-selectively ionized, probed with velocity-map imaging (VMI), and filtered on the basis of momentum conservation (*22*). Such coincident detection was used to characterize the 2KRb → K_2 + Rb_2 process with full state-to-state resolution. The energy release in the KRb reaction (≈10 cm^{-1}) is partitioned between the rotational and translational energies of the product K_2 and Rb_2 molecules, permitting the K_2 and Rb_2 molecular rotation to be excited up to $N_{K_2} = 12$ and $N_{Rb_2} = 20$. A comprehensive study of the product state space revealed a distribution predominantly proportional to the degeneracy of each product state channel, implying that the underlying dynamics are chaotic (*22*). Nevertheless, reaction products have been controlled by reactant nuclear spins (*23*), in a manner that indicates the conservation of nuclear spin populations in such a reaction. This fact positions the nuclear spin degree of freedom as a promising candidate for the study of quantum coherence and entanglement within chemical reactions. We note that the role of coherence was not explored in (*23*) because the state-resolved reaction outcomes were averaged rather than coincidentally detected.

Interference pattern in reaction-product distribution

In this study, we investigated whether coherence was maintained within the nuclear spin degree of freedom throughout an atom-exchange reaction. We designed an experiment with reactants prepared in an entangled nuclear spin state and measured the outcome to distinguish between coherent and incoherent processes (Fig. 1). If coherence is maintained, it will become evident in the final-product nuclear spin state distribution. However, detecting the product-molecule nuclear spin state spectroscopically is generally challenging because of small energy splittings compared with the natural linewidth of the transitions and Doppler shifts from the fast-flying products. Instead, we indirectly probed the nuclear spin degree of freedom, making use of the symmetry of the nuclear spin states and the parity of the orbital wave function and how they respect the exchange symmetry of the two indistinguishable nuclei (*24*) in the homonuclear diatomic product molecules K_2 and Rb_2. Specifically, the nucleus of ^{40}K (^{87}Rb) is bosonic (fermionic), and thus the total nuclear wave function of K_2 (Rb_2), which can be factored into a spin part and a spatial part, is symmetric (antisymmetric) under exchange (*23*) (Fig. 1A). By probing the parity, even or odd, of the rotational states of the outgoing products, we obtained the symmetry of the product nuclear spins.

Previous work suggests that the nuclear spin dynamics in the reaction process could be described by transforming the two nuclear spins in K or Rb (in two separate KRb molecules) from the uncoupled basis to the coupled basis in K_2 or Rb_2 (*23*). Assuming that the nuclear spin wave functions remained coherent throughout the reaction, coupling two K or two Rb with the same spin projection led only to a symmetric total spin state, $|S\rangle$. Coupling two K or two Rb with different spin projections resulted in a superposition of $|S\rangle$ and $|A\rangle$ (A is antisymmetric), where the relative phase depended on the coupling order, causing interference between different reaction pathways (*25*) [also see supplementary materials (SM) section S1]. Consequently, destructive interference led to complete suppression of the $|K_2\rangle^{nuc} \otimes |Rb_2\rangle^{nuc} = |S\rangle \otimes |A\rangle$ and the $|A\rangle \otimes |S\rangle$ channels (Fig. 1B). Owing to the spin-rotation correspondence of the K_2 and Rb_2 nuclei, the product states $|e,e\rangle$ and $|o,o\rangle$, where e is an even-numbered and o is an odd-numbered rotation state, were also completely suppressed, and the population was entirely in the $|e,o\rangle$ and $|o,e\rangle$ channels. Both the spin and the rotational components of the K_2 and Rb_2 molecule wave functions became entangled because they inherited the entanglement from the reactants (*26*). By contrast, if the nuclear spin states were no longer pure because of decoherence occurring either before or during the reaction, the two K and Rb nuclei were no longer indistinguishable and the symmetry protection was lost. As a consequence, the $|S,A\rangle(|e,e\rangle)$ and $|A,S\rangle(|o,o\rangle)$ channels would be populated

[1]Department of Chemistry and Chemical Biology, Harvard University, Cambridge, MA 02138, USA. [2]Harvard-MIT Center for Ultracold Atoms, Cambridge, MA 02138, USA. [3]Institut für Experimentalphysik, Universität Innsbruck, 6020 Innsbruck, Austria. [4]Department of Physics, Harvard University, Cambridge, MA 02138, USA.
*Corresponding author. Email: ni@chemistry.harvard.edu
†These authors contributed equally to this work.
‡Present address: QuEra Computing, Boston, MA 02135, USA.

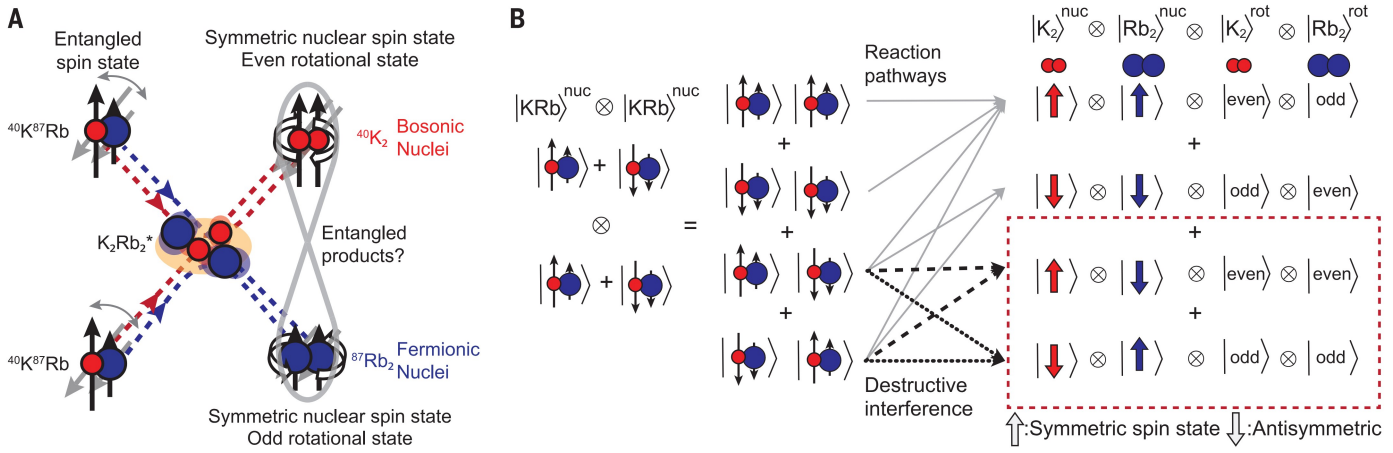

Fig. 1. Atom-exchange reaction with reactant molecules prepared in entangled nuclear spin states yields distinct product outcomes depending on whether the reaction preserves coherence or not. (**A**) Reaction of interest. Would entangled nuclear spins in the reactant KRb molecule result in entangled products of K_2 and Rb_2? Because of the exchange symmetry of indistinguishable nuclei in homonuclear diatomic molecules (K_2 and Rb_2), the symmetry of the nuclear spins can be probed through the parity of the rotation states. (**B**) If the nuclear spin wave function stays coherent throughout the reaction, reaction pathways destructively interfere for the $|S, A, e, e\rangle$ and $|A, S, o, o\rangle$ channels. If the nuclear spin wave function decoheres into a statistical mixture, either before or during the chemical reaction, no interference between the bottom two paths exists, and all four product channels will be populated.

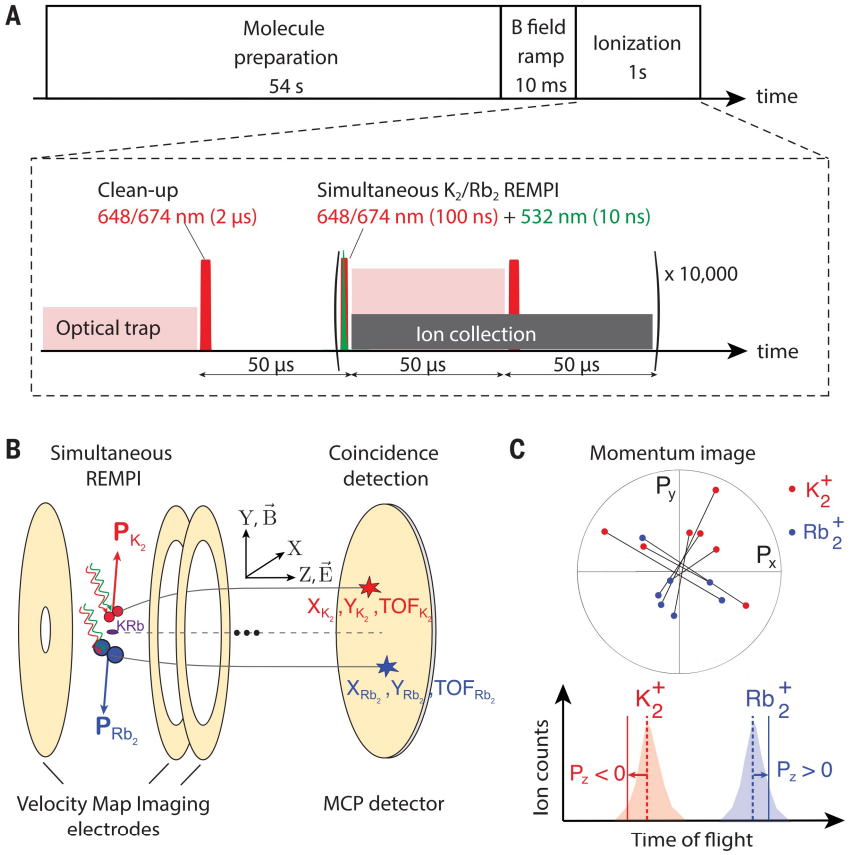

Fig. 2. Coincidence detection of reaction products. (**A**) Experimental timing sequence highlighting reaction-product ionization detection. The optical dipole trap (ODT) was modulated at a 10-kHz rate with a 50% duty cycle. At the beginning of each ODT dark period, a cleanup pulse consisting of 648- and 674-nm beams was added to remove the K_2 and Rb_2 products formed while the ODT was on. At the end of the ODT dark period, we simultaneously turned on K_2 and Rb_2 resonance-enhanced multiphoton ionization (REMPI) pulses and started ion collection for 95 μs. We repeated the ionization detection 10,000 times for each experimental cycle. (**B**) Quantum-state selective ionization and coincidence detection setup. Product K_2 and Rb_2 molecules were ionized simultaneously by REMPI pulses targeted at specific quantum states. Ions were accelerated by electrodes arranged in velocity-map imaging (VMI) configuration. The microchannel plate (MCP) detector recorded the position and the arrival time-of-flight (TOF) of the ions that were used for filtering the coincidence ion pairs. (**C**) Coincidence K_2^+-Rb_2^+ pair filtering. Products from the same reaction event must satisfy the momentum conservation criteria $\mathbf{P}_{K_2} + \mathbf{P}_{Rb_2} = 0$. The momentum components perpendicular to the TOF axis (z axis), P_x and P_y, were mapped onto the impact positions on the MCP detector. The momentum component along the TOF axis, P_z, was mapped on the TOF. The details of the momentum filter are in SM section S3.

in addition to the $|S,S\rangle(|e,o\rangle)$ and $|A,A\rangle(|o,e\rangle)$ channels. Inspecting the population distribution of the four parity channels provides a feasible way to test whether coherence was preserved.

Coherent chemical reactions with reactant KRb molecules in an entangled spin state

Our experiment started with the preparation of ultracold rovibrational ground-state $^{40}K^{87}Rb$ molecules in a single hyperfine state at 500 nK. The molecular gas was trapped in an optical dipole trap (ODT) in an apparatus with ion spectrometry and velocity map imaging (*27*). The entangled KRb state could be prepared relatively easily by magnetic field ramping

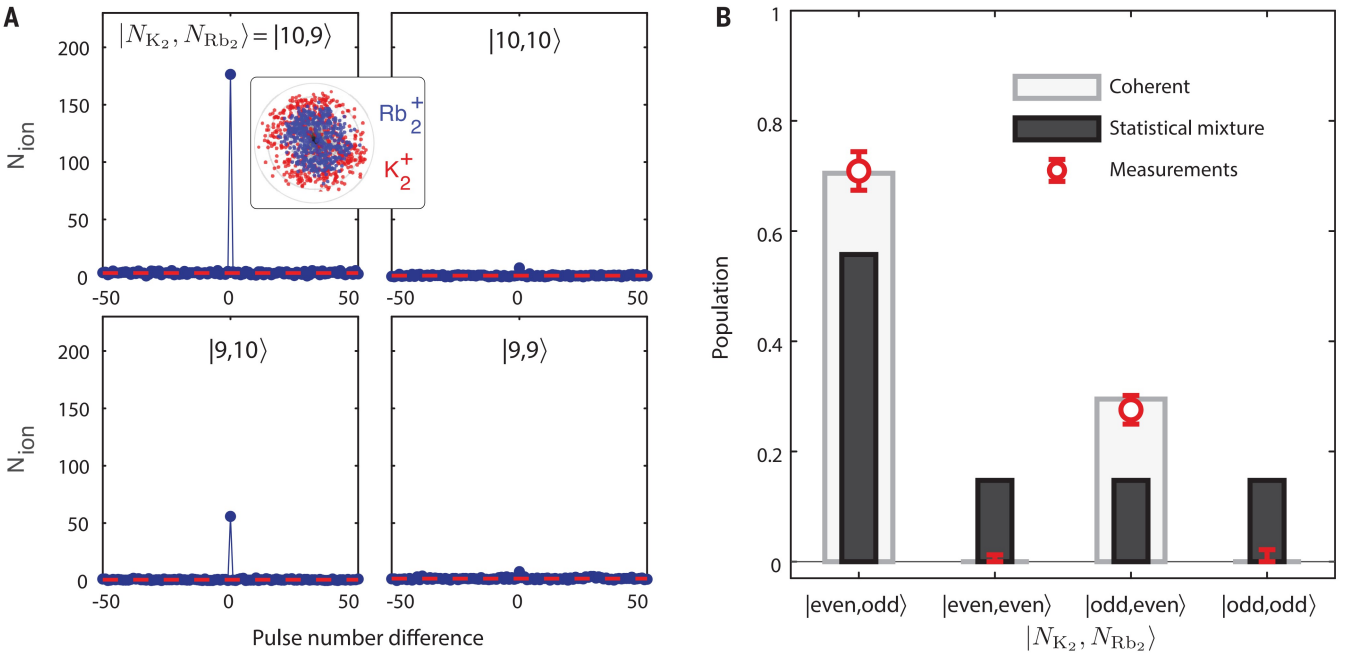

Fig. 3. Coherent reaction product-state distribution. (**A**) K_2^+-Rb_2^+ coincidence pair counts per 1000 cycles for each $|N_{K_2}, N_{Rb_2}\rangle$ after momentum filtering along all three directions as a function of pulse-number difference between the two ions. A pulse-number difference of 0 means that the K_2^+ and Rb_2^+ are generated by simultaneous ionization. The finite background ion pair counts in $|10,10\rangle$ and $|9,9\rangle$ are further explained in the main text. The background data are shown in fig. S1. (Inset) $|10,9\rangle$ pair velocity-map image on the *xy* plane. (**B**) The normalized measured population of each parity channel after background subtraction of the products (red data) overlaid on the expected K_2 and Rb_2 rotational-state population distributions: If the nuclear spin wave function remains pure, the population distribution follows the light-gray bars; if the nuclear spin wave function fully dephases, the expected distribution is represented by the solid black and gray bars. The P_{eo} and P_{oe} error bars are propagated from the standard deviation of shot noise of the $|10,9\rangle$ and $|9,10\rangle$ coincidence counts; the P_{oo} and P_{ee} ranges are propagated from the 68% confidence intervals of the $|9,9\rangle$ and $|10,10\rangle$ count rates after background subtraction with Bayesian analysis. The measured results align well with the fully coherent case, indicating that the nuclear spins stay coherent throughout the reaction.

because of the interaction between the two nuclei in KRb. We started with KRb in state $|\psi_i\rangle = |N, m_N, m_I^K, m_I^{Rb}\rangle = |0,0,-4,1/2\rangle$ at 542 G, where N is the rotational quantum number, m_N is the rotation projection, and m_I^K (m_I^{Rb}) is the K (Rb) nuclear spin projection along the quantization axis. We then ramped the magnetic field to 5 G within 10 ms. Throughout the field ramp, the KRb molecules remained in an energy eigenstate (SM section S4) and ended in the state

$$|\psi_f\rangle = \alpha|0,0,-4,1/2\rangle + \beta|0,0,-3,-1/2\rangle + \gamma|0,0,-2,-3/2\rangle \quad (1)$$

where $(\alpha,\beta,\gamma) = (0.595, 0.719, 0.359)$ at 5 G and the K nuclear spin and the Rb nuclear spin were entangled. The $2KRb \rightarrow K_2 + Rb_2$ reaction occurs continuously through collisions. We strobed the ODT on and off at a 10-kHz repetition rate, which allowed us to probe products formed in the dark, thereby minimizing any perturbations from the ODT. The reaction products formed in the presence of the ODT were removed by cleanup pulses (Fig. 2A).

If the coherence is preserved (Fig. 1B), we expect the populations in the different rotational parity channels to be

$$P_C \equiv \begin{bmatrix} P_{eo} & P_{ee} \\ P_{oo} & P_{oe} \end{bmatrix} = \begin{bmatrix} 1-x & 0 \\ 0 & x \end{bmatrix} = \begin{bmatrix} 0.7049 & 0 \\ 0 & 0.2951 \end{bmatrix} \quad (2)$$

where $x = |\alpha\beta|^2 + |\beta\gamma|^2 + |\alpha\gamma|^2$ (SM section S1). In this case, P_{eo} refers to the population fraction with even K_2 and odd Rb_2 rotational quantum numbers. P_{oe}, P_{ee}, and P_{oo} are defined analogously, and all four populations add to 1. If the nuclear spin state decoheres into a statistical mixture, we expect

$$P_S \equiv \begin{bmatrix} 1-\frac{3}{2}x & \frac{1}{2}x \\ \frac{1}{2}x & \frac{1}{2}x \end{bmatrix} = \begin{bmatrix} 0.5575 & 0.1475 \\ 0.1475 & 0.1475 \end{bmatrix} \quad (3)$$

Coincident detection is required to distinguish between the coherent and statistical mixture outcomes because noncoincident detection would only be sensitive to the sum of the other product (e.g., $P_{N_{K_2}=\ even} = P_{eo} + P_{ee}$). Experimentally, we restricted ourselves to the state pairs $|N_{K_2}, N_{Rb_2}\rangle$ = $|10,9\rangle$, $|10,10\rangle$, $|9,10\rangle$, and $|9,9\rangle$ because of their higher signal compared with other channels. Additionally, the degeneracy of the $|10,9\rangle$ pair is well described by the statistical model (*22*), which is essential for proper normalization.

We probed the population of molecules in each rotation state using simultaneous state-selective resonance-enhanced multiphoton ionization (REMPI) of K_2 and Rb_2, following (*22*, *23*) (SM section S2) and a timing sequence shown in Fig. 2A. The ions were accelerated by electrodes arranged in the VMI configuration and collected by a time- and position-sensitive microchannel plate (MCP) detector (Fig. 2B). For each experimental cycle (cycle time of 55 s), we probed the reaction products for 1 s. We accumulated data for ~3000 cycles (~46 hours) for each state pair. Momentum conservation ensured that the total momentum of the K_2 and Rb_2 molecules originating from the same reaction events remained zero because the reactants started with near zero momentum. We filtered the momentum along the time-of-flight (TOF) axis (z axis) using the TOF and additionally the momentum along x and y directions using MCP position information

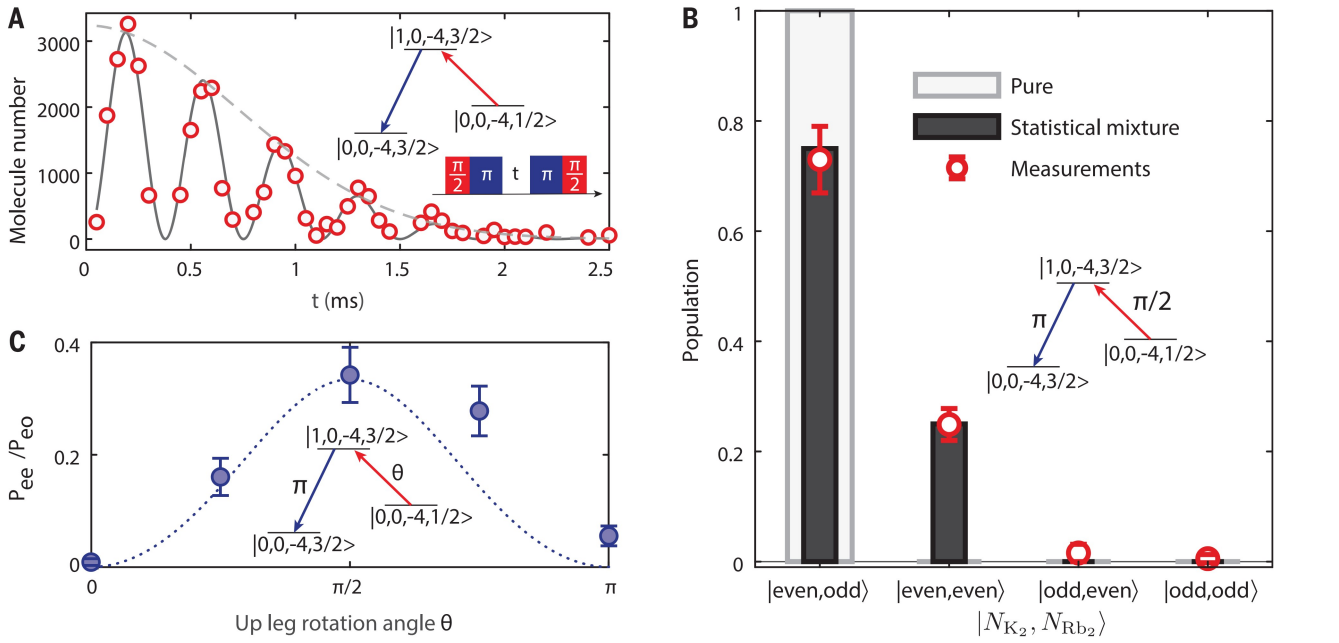

Fig. 4. Reaction with reactant molecules prepared in a statistical mixture. (**A**) Ramsey spectroscopy of KRb molecules in the superposition of two hyperfine states, $|0,0,-4,1/2\rangle$ and $|0,0,-4,3/2\rangle$, prepared by two consecutive microwave pulses (scheme and timing shown in the inset). The solid line is a fitting of molecule number to a damped oscillation with a Gaussian decay envelope. The dashed line is the fitted envelope $\exp\left(-(t/T_2)^2\right)$, from which T_2 = 1.03(6) ms is extracted. (**B**) Comparison of the measured population of the four $|N_{K_2}, N_{Rb_2}\rangle$ state pairs (open red circles) versus the expectation for the pure and statistical-mixture outcomes. The data are taken with reactants prepared in a 50-50 mixture of $|0,0,-4,1/2\rangle$ and $|0,0,-4,3/2\rangle$. Error bars are propagated from the standard deviation of the shot noise of each state pair's coincidence counts. The solid black and gray bars are the expected population for a completely decohered state, and the light-gray bars show the expected population distribution for a pure initial state $\frac{1}{\sqrt{2}}|0,0,-4,1/2\rangle + \frac{1}{\sqrt{2}}|0,0,-4,3/2\rangle$. (**C**) Controlling the population between $|e,e\rangle$ and $|e,o\rangle$ channels by tuning the population ratio in the statistical mixture of $|0,0,-4,1/2\rangle$ and $|0,0,-4,3/2\rangle$. The population of the $|0,0,-4,1/2\rangle$ state is $\cos^2(\frac{\theta}{2})$, and the population of $|0,0,-4,3/2\rangle$ is $\sin^2(\frac{\theta}{2})$, where θ is the up-leg rotation angle. The dotted line is the theory calculation of the P_{ee}/P_{eo} (following Eq. 5) overlaid on data (blue circles), where the error bars are propagated from the standard deviation of the shot noise on the $|10,10\rangle$ and $|10,9\rangle$ coincidence counts. The deviation of the measurements from the dotted line at large rotation angles could be attributed to imperfect state preparation.

from VMI for all collected reaction events to extract coincidence counts of each of the product state pairs (Fig. 2C and SM section S3). The accumulated coincidence-count rates of the four state pairs (Fig. 3A) are $\begin{bmatrix} N_{|10,9\rangle} & N_{|10,10\rangle} \\ N_{|9,9\rangle} & N_{|9,10\rangle} \end{bmatrix} = \begin{bmatrix} 173.1\pm8 & 6.7\pm1.8 \\ 6.1\pm1.8 & 55.2\pm4.2 \end{bmatrix}$, where error bars represent shot noise. The coincidence counts of $|10,10\rangle$ and $|9,9\rangle$ could represent decoherence or could emerge from other sources, such as the ionization of other state pairs. This scenario might occur when one product was ionized through state-selective REMPI and the other product was off-resonantly ionized by two 532-nm photons, which could register as a coincident count during data accumulation.

To quantify such a background contribution, we detected the $|10,10\rangle$ channel at 50 G, where the KRb was dominantly in $|0,0,-4,1/2\rangle$ (with 0.994 population), and we did not expect any reaction outcome in $|10,10\rangle$. In this background measurement, we found a coincidence-count rate of 7.1 ± 1.7, which could account for the entire contribution to the measured $|10,10\rangle$ and $|9,9\rangle$ counts at 5 G. Additionally, we looked for counts that came from both products being off-resonantly ionized by turning off the resonant legs of the REMPI beams and found them negligible.

For the $|10,9\rangle$ and $|9,10\rangle$ channels, we simply subtracted this background source from the measured signal. For the $|10,10\rangle$ and $|9,9\rangle$ channels, because the measured signal was lower than the measured background because of random fluctuations, we used Bayesian analysis (*28*) to find the 68% confidence intervals. We then normalized all channels, accounting for the velocity factors and channel degeneracies (SM section S5), to extract the branching ratios $\begin{bmatrix} P_{eo} & P_{ee} \\ P_{oo} & P_{oe} \end{bmatrix} = \begin{bmatrix} 0.709\pm0.035 & [0,0.007] \\ [0,0.012] & 0.276\pm0.026 \end{bmatrix}$. These measurements (Fig. 3B) were near the coherent values of P_C (Eq. 2).

To further quantify the degree of coherence in the uncoupled spin basis that was preserved in this reaction, we assumed a dephasing model [because previous work in (*23*) established population conservation] in which all the off-diagonal terms in the density matrix decay by an equal amount. As such, we multiplied the off-diagonals of the initial pure-state KRb + KRb spin-density matrix by a common factor, Γ, to find the decohered spin-density matrix of the reaction products

$$\rho_{K_2,Rb_2} = \Gamma U \rho_{KRb} \otimes \rho_{KRb} U^\dagger + (1-\Gamma) U (\rho_{KRb} \otimes \rho_{KRb})_{diag} U^\dagger \quad (4)$$

where $\rho_{KRb} = |\psi_f\rangle\langle\psi_f|$, U is the unitary transformation that transforms the two K and Rb nuclear spins from uncoupled basis to coupled basis, and $(\rho_{KRb} \otimes \rho_{KRb})_{diag}$ is the diagonal part of the pure-state density matrix $\rho_{KRb} \otimes \rho_{KRb}$. With these assumptions, the final branching ratio could be described by $\Gamma P_C + (1-\Gamma)P_S$. From Bayesian analysis (SM section S6), we found that the result, in the space of detected products, was consistent with full coherence ($\Gamma = 1$) and no lower than 0.9014 (95% confidence interval), limited by data statistics. These results showed that the nuclear spin wave function remained coherent throughout the reaction. Assuming that the rotational states also stayed coherent, we could further infer that the nuclear spin states of K_2 and Rb_2 molecules, along with their rotational states, were entangled. Intriguing questions

regarding the direct verification and the lifetime of the entanglement after the products separate were beyond the scope of this study.

Controlling the product-state distribution with decoherence

As we found the initial reactant state $|\psi_f\rangle$ (Eq. 1) to be robust to decoherence, both from experimental noise and chemical reaction, we could not contrast the coherent outcome with that of a statistical mixture by letting the state decohere. Thus, we deliberately prepared the reactants in a statistical mixture of two energy eigenstates, $|0,0,-4,1/2\rangle$ and $|0,0,-4,3/2\rangle$, through the intermediate state $|1,0,-4,3/2\rangle$, using sequential microwave pulses (Fig. 4A, inset). The ambient magnetic and electric field were set to 200 G and 424 V/cm, where the microwave transitions were sufficiently isolated from neighboring ones. By applying an up-leg pulse with rotation angle θ on the Bloch sphere and a down-leg π pulse, we created a superposition state $\cos(\theta/2)|0,0,-4,1/2\rangle+\sin(\theta/2)|0,0,-4,3/2\rangle$. We characterized the coherence decay using Ramsey spectroscopy and found a Gaussian decay envelope with a 1.03(6)-ms time constant (Fig. 4A). This time scale was much shorter than the *p*-wave collision time of ~250 ms (fig. S3) for indistinguishable fermionic KRb molecules measured under our experimental conditions. Therefore, the reaction process was dominated by *s*-wave reactions between distinguishable KRb molecules, which proceed ~100 times faster than the *p*-wave collision rate (*20*). Following the procedure used to produce Eq. 2 and 3, it can be shown that the expected population distribution for this statistical mixture is

$$\begin{bmatrix} P_{eo} & P_{ee} \\ P_{oo} & P_{oe} \end{bmatrix} = \begin{bmatrix} 1-y & y \\ 0 & 0 \end{bmatrix} \quad (5)$$

where $y=\sin^2\left(\frac{\theta}{2}\right)\cos^2\left(\frac{\theta}{2}\right)$ and the emergence of e, e is a result of decoherence. For a 50-50 statistical mixture ($\theta=\pi/2$) of $|0,0,-4,1/2\rangle$ and $|0,0,-4,3/2\rangle$, the measured branching ratio of the four states is shown in Fig. 4B, aligning well with the expected values in Eq. 5 and demonstrating control of the reaction products when using decoherence. Furthermore, by tuning the population ratio between the $|0,0,-4,1/2\rangle$ and $|0,0,-4,3/2\rangle$ states, the reaction-product distribution agreed with the theoretical predictions (Fig. 4C).

Summary

We investigated the fundamental question of whether coherence could be preserved in reactive scattering using a model atom-exchange reaction that proceeded in a well-isolated gas phase setup. We examined specifically the nuclear spin degree of freedom by preparing entangled nuclear spins in reactants and measuring product outcomes. Similarly to Hong-Ou-Mandel interference of indistinguishable particles (*29*–*32*), the coherent phase information was mapped onto the outcome population distribution, manifested as destructive interference of the $|e,e\rangle$ and $|o,o\rangle$ channels. By measuring the populations of each parity channel, we observed that coherence of the nuclear spin wave function was preserved, which suggested that the products were in an entangled state $\sqrt{P_{eo}}|S,S\rangle|e,o\rangle+\sqrt{P_{oe}}|A,A\rangle|o,e\rangle$. However, direct characterization of the relative phase in the product quantum state would require future measurements in a different basis (*33*), in which driving even-to-odd rotational transitions and resolving individual nuclear spin states of K_2 and Rb_2 molecules would be necessary.

Although this work is reminiscent of hyperfine spin entanglement generated in atomic collisions (*34*–*36*), the persistence of nuclear spin coherence in the presence of short-range interactions during chemical reactions, which typically couple different degrees of freedom, is unexpected. Our work shows that a reaction that exchanges atom partners could be a resource to generate entangled pairs, allowing trivial entanglement to be separated and rearranged into parting molecules—a strategy that could be extended to various other chemical processes, such as molecular qubits built from chemical synthesis (*37*). Lastly, our findings precede the study of coherence in reactions under wet and warm conditions, which may be of interest for a wide range of chemical phenomena, including in the brain (*38*).

REFERENCES AND NOTES

1. D. Akoury *et al.*, *Science* **318**, 949–952 (2007).
2. H. Zhou, W. E. Perreault, N. Mukherjee, R. N. Zare, *Science* **374**, 960–964 (2021).
3. P. G. Jambrina *et al.*, *Nat. Chem.* **7**, 661–667 (2015).
4. Y. Xie *et al.*, *Science* **368**, 767–771 (2020).
5. W. Chen *et al.*, *Science* **371**, 936–940 (2021).
6. M. Shapiro, P. Brumer, *Phys. Rev. Lett.* **77**, 2574–2576 (1996).
7. S. S. Kale, Y. P. Chen, S. Kais, *J. Chem. Theory Comput.* **17**, 7822–7826 (2021).
8. D. B. Blasing *et al.*, *Phys. Rev. Lett.* **121**, 073202 (2018).
9. L. Zhu *et al.*, *Science* **270**, 77–80 (1995).
10. B. Sheehy, B. Walker, L. F. DiMauro, *Phys. Rev. Lett.* **74**, 4799–4802 (1995).
11. A. Shnitman *et al.*, *Phys. Rev. Lett.* **76**, 2886–2889 (1996).
12. K.-K. Ni *et al.*, *Science* **322**, 231–235 (2008).
13. J. G. Danzl *et al.*, *Science* **321**, 1062–1066 (2008).
14. F. Lang, K. Winkler, C. Strauss, R. Grimm, J. H. Denschlag, *Phys. Rev. Lett.* **101**, 133005 (2008).
15. L. W. Cheuk *et al.*, *Phys. Rev. Lett.* **121**, 083201 (2018).
16. M. R. Tarbutt, *Contemp. Phys.* **59**, 356–376 (2018).
17. Y. Wu, J. J. Burau, K. Mehling, J. Ye, S. Ding, *Phys. Rev. Lett.* **127**, 263201 (2021).
18. T. K. Langin, V. Jorapur, Y. Zhu, Q. Wang, D. DeMille, *Phys. Rev. Lett.* **127**, 163201 (2021).
19. M.-G. Hu *et al.*, *Science* **366**, 1111–1115 (2019).
20. S. Ospelkaus *et al.*, *Science* **327**, 853–857 (2010).
21. Y. Liu *et al.*, *Nat. Phys.* **16**, 1132–1136 (2020).
22. Y. Liu *et al.*, *Nature* **593**, 379–384 (2021).
23. M.-G. Hu *et al.*, *Nat. Chem.* **13**, 435–440 (2021).
24. R. Feynman, R. Leighton, M. Sands, *The Feynman Lectures on Physics*, vol. III (Addison Wesley, 1965).
25. G. Quéméner *et al.*, *Phys. Rev. A* **104**, 052817 (2021).
26. If the initial KRb nuclear spin state is a product state of K and Rb nuclear spins and remains pure, regardless of their specific components, the resulting K_2 and Rb_2 molecules will always exhibit e,o because of symmetry protection.
27. Y. Liu, D. D. Grimes, M.-G. Hu, K.-K. Ni, *Phys. Chem. Chem. Phys.* **22**, 4861–4874 (2020).
28. R. J. Little, *Health Phys.* **43**, 693–703 (1982).
29. C. K. Hong, Z. Y. Ou, L. Mandel, *Phys. Rev. Lett.* **59**, 2044–2046 (1987).
30. A. M. Kaufman *et al.*, *Science* **345**, 306–309 (2014).
31. S. Ramelow, L. Ratschbacher, A. Fedrizzi, N. K. Langford, A. Zeilinger, *Phys. Rev. Lett.* **103**, 253601 (2009).
32. A. Fedrizzi *et al.*, *New J. Phys.* **11**, 103052 (2009).
33. M. A. Nielsen, I. L. Chuang, *Quantum Computation and Quantum Information* (Cambridge Univ. Press, 2010).
34. A. Sørensen, L.-M. Duan, J. I. Cirac, P. Zoller, *Nature* **409**, 63–66 (2001).
35. J. Estève, C. Gross, A. Weller, S. Giovanazzi, M. K. Oberthaler, *Nature* **455**, 1216–1219 (2008).
36. C. D. Hamley, C. Gerving, T. Hoang, E. Bookjans, M. S. Chapman, *Nat. Phys.* **8**, 305–308 (2012).
37. M. R. Wasielewski *et al.*, *Nat. Rev. Chem.* **4**, 490–504 (2020).
38. M. P. Fisher, *Ann. Phys.* **362**, 593–602 (2015).
39. Y.-X. Liu *et al.*, Data for Quantum Interference and Entanglement in Atom-Exchange Reactions, version 2.0, Harvard Dataverse (2024); http://dx.doi.org/10.7927/H4M61H5F.

ACKNOWLEDGMENTS

We thank T. Rosenband for Bayesian data analysis and F. Ferlaino and the BEC2023 community for discussions. **Funding:** This work is funded primarily by NSF-EAGER through grant CHE-2332539; the Gordon and Betty Moore Foundation through grant GBMF11558; the David and Lucile Packard Foundation, U.S. Department of Energy (DOE), Office of Science, Basic Energy Sciences (BES), under award no. DE-SC0024087; and the Center for Ultracold Atoms (an NSF Physics Frontiers Center). A.H. acknowledges funding from the Austrian Science Fund (FWF) within the DK-ALM (grant no. W1259-N27). **Author contributions:** K.-K.N. and M.-G.H. conceived the idea. Y.-X.L. and L.Z. developed the idea, carried out the experiments, and analyzed data. J.L., J.J.A.H., and M.C.B. contributed to data collection and analysis. K.-K.N. supervised this project and analyzed data. All authors contributed to interpreting the results and writing the manuscript. **Competing interests:** The authors declare that they have no competing interests. **Data and materials availability:** All data needed to evaluate the conclusions in the paper are present in the paper or the supplementary materials. All data presented in this paper are available at Harvard Dataverse (*39*).

SUPPLEMENTARY MATERIALS

science.org/doi/10.1126/science.adl6570
Supplementary Text
Figs. S1 to S4
Tables S1 and S2
References (*40*–*45*)

Submitted 14 November 2023; accepted 19 April 2024
Published online 16 May 2024
10.1126/science.adl6570